

See discussions, stats, and author profiles for this publication at: <https://www.researchgate.net/publication/260721456>

Exotic magnetism of s-electron cluster arrays: Ferromagnetism, ferrimagnetism and antiferromagnetism

Article in Journal- Korean Physical Society · August 2013

DOI: 10.3938/jkps.63.699

CITATIONS

5

READS

23

6 authors, including:



Takehito Nakano

Osaka University

71 PUBLICATIONS 483 CITATIONS

SEE PROFILE



Yasuo Nozue

Osaka University

130 PUBLICATIONS 1,684 CITATIONS

SEE PROFILE



Nguyen Hoang Nam

Hanoi University of Science

39 PUBLICATIONS 300 CITATIONS

SEE PROFILE



Truong Cong Duan

Osaka University

5 PUBLICATIONS 41 CITATIONS

SEE PROFILE

Some of the authors of this publication are also working on these related projects:



Application of gold nanoparticles in virus detection biosensor [View project](#)



Synthesis and applications of multifunctional nanoparticles in biomedicine [View project](#)

Exotic Magnetism of s -electron Cluster Arrays: Ferromagnetism, Ferrimagnetism and Antiferromagnetism

Takehito NAKANO, Duong Thi HANH and Yasuo NOZUE*

Department of Physics, Graduate School of Science, Osaka University, Osaka 560-0043, Japan

Nguyen Hoang NAM

*Center for Materials Science, Faculty of Physics,
Hanoi University of Science, VNU, Hanoi, Vietnam*

Truong Cong DUAN

Department of Research and Development Program, FPT University, Hanoi, Vietnam

Shingo ARAKI

Graduate School of Natural Science and Technology, Okayama University, Okayama 700-0082, Japan

(Received 5 June 2012, in final form 1 October 2012)

Alkali metal nanoclusters can be stabilized in the regular cages of zeolite crystals by the loading of guest alkali metals. Cages are connected by the sharing of windows of the framework, and arrayed in simple cubic, diamond and body centered cubic structures in zeolites A, X and sodalite, respectively. The s -electrons have the localized nature of nanoclusters with magnetic moments, and have mutual interactions through the windows of cages. They show exotic magnetism depending on the structure type of zeolites, the kind of alkali metals and the average loading density of alkali atoms per cage. In zeolite A, potassium clusters are formed in α -cages that have an inside diameter of 11 Å. They exhibit ferromagnetic properties explained by the canted antiferromagnetism of the Mott insulator, where the $1p$ -like degenerate orbitals of clusters play an essential role in the magnetic properties. Na-K alloy clusters generated at supercages and β -cages of low-silica X (LSX) zeolite exhibit Néel's N-type ferrimagnetism at specific loading densities of alkali metals. Alkali metal clusters in sodalite show the ideal Heisenberg antiferromagnetism of the Mott insulator.

PACS numbers: 75.50.Gg, 75.50.Ee, 71.38.-k, 76.50.+g, 75.70.Tj, 75.20.Hr, 82.75.Vx

Keywords: Alkali metal, Cluster, Ferromagnetism, Ferrimagnetism, Antiferromagnetism, Zeolite, Spin orbit interaction, Nanomaterial, Superatom

DOI: 10.3938/jkps.63.699

I. INTRODUCTION

Non-magnetic elements of the alkali metals only show weak magnetism, such as Pauli's paramagnetism of free electrons. When s -electrons of alkali metals are confined in nanoparticles, they can have localized magnetic moments depending on the number of electrons and temperature [1]. If we can make such nanoclusters (nanoparticles) with homogeneous size and regular periodicity for mutual interaction, nanoclusters are expected to acquire exotic magnetism without including magnetic elements. In order to make arrays of alkali-metal nanoclusters, we have employed nanoporous crystals of zeolites as the host materials. In zeolite crystals, regular nanocages are ar-

rayed in three-dimension and are connected by the sharing of windows. New s -electron systems can be constructed by the loading of guest alkali metals into zeolite crystals. Many different zeolite crystals are available for the loading of guest alkali metals, such as zeolite A (LTA), LSX (FAU), sodalite (SOD), *etc.*, where the three characters in parentheses stand for the framework structure codes given by IUPAC.

Zeolite A is a typical aluminosilicate zeolites. As shown schematically in Fig. 1(a), truncated octahedral β -cages are arrayed in a simple cubic structure by the sharing of cubes. Among them, truncated cuboctahedral α -cages are formed. The α -cages are arrayed in a simple cubic structure by the sharing of windows of 8-membered-rings (8MRs); β - and α -cages are arrayed in a CsCl structure. The aluminosilicate framework ($\text{Al}_{12}\text{Si}_{12}\text{O}_{48}$ per β - or α -cage) is negatively charged by

*E-mail: nozue@phys.sci.osaka-u.ac.jp

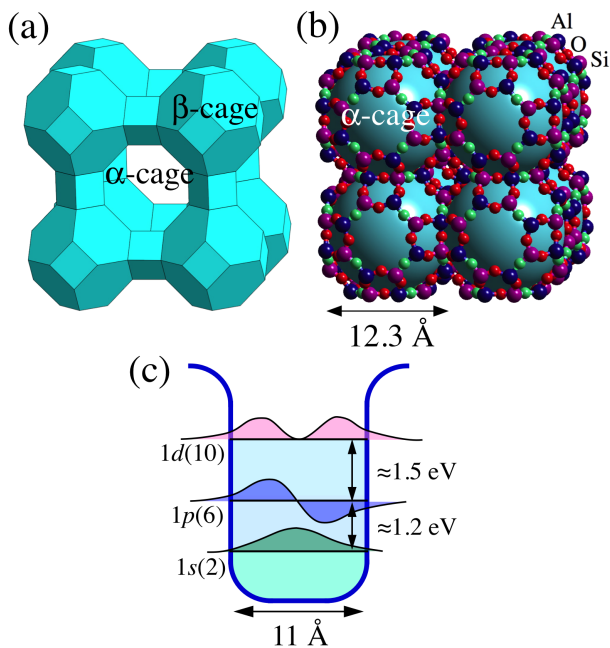


Fig. 1. (Color online) (a) Polyhedral illustration of aluminosilicate zeolite A (LTA framework structure), and (b) alkali-metal clusters stabilized in α -cages of zeolite A. (c) Spherical-well potential model for s -electrons confined in α -cage. Quantum states $1s$, $1p$ and $1d$ appear in increasing order of energy, and have a finite overlap with adjacent clusters.

Al atoms. Exchangeable positive ions (cations) are distributed in the space of the framework for charge neutrality. The s -electrons provided by the loading of guest alkali metals are shared with many zeolite cations. These s -electrons are confined by the negatively-charged framework to form cationic clusters. In the case of loading guest potassium metal into K-cation-type zeolite A (abbreviated to K_{12} -A here), cationic clusters are stabilized in α -cages as shown in Fig. 1(b). Large spheres illustrate the s -electron wave functions of clusters stabilized in α -cages. Zeolite K_{12} -A loaded with the average number of guest K atoms, n , is abbreviated to K_n/K_{12} -A here, and has the chemical formula $K_{12+n}Al_{12}Si_{12}O_{48}$. The loading density n corresponds to the average number of s -electrons per cage. If we simplify the effective potential for guest s -electrons to a spherical one with the size of the effective inside diameter of the α -cage, ≈ 11 Å, quantum states $1s$, $1p$ and $1d$ appear in increasing order of energy, as illustrated in Fig. 1(c). The first two electrons occupy the $1s$ state, and next six electrons the $1p$ state, etc., as in superatoms. The energy intervals between $1s$ - $1p$ and $1p$ - $1d$ are calculated to be ≈ 1.2 and ≈ 1.5 eV, respectively.

An optical absorption band appears at 1.2 eV in the dilutely K-loaded K_{12} -A, and is assigned to the $1s$ - $1p$ allowed transition [2]. Optical reflection bands at higher loading densities have been assigned to $1s$ - $1p$ and $1p$ - $1d$ allowed transitions [2]. The most striking property of

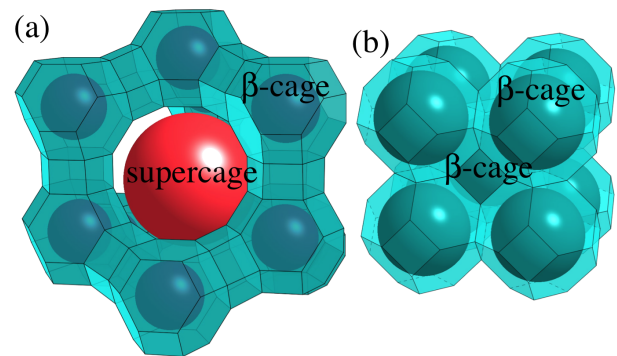


Fig. 2. (Color online) Schematic illustration of (a) alkali-metal clusters stabilized in β -cages and supercages of LSX zeolite having FAU framework structure, and of (b) alkali-metal clusters stabilized in β -cages of sodalite having SOD framework structure.

K-loaded K_{12} -A is ferromagnetic behavior although no magnetic element is contained [3]. Ferromagnetic properties vary systematically with the average loading density [4]. The finite optical gap is observed in the infrared spectral region, indicating that these materials are Mott insulators [5]. The origin of the spontaneous magnetization is explained by the spin-canting mechanism of antiferromagnet [6], where the spin-orbit interaction is strongly enhanced by the degeneracy of the $1p$ orbital in the presence of many K-cations [7–10]. In Rb-loaded Rb_{12} -A, clusters are formed at both α - and β -cages at higher loading densities, and show spontaneous magnetization [11–13]. This magnetic phase is assigned to ferrimagnetism of two nonequivalent magnetic sublattices of α - and β -cages.

Zeolite X with the highest Al-concentration of framework ($Si/Al = 1$) is called low-silica X (abbreviated to LSX) zeolite. In zeolite LSX (or X), β -cages are arrayed in a diamond structure by the sharing of double 6-membered-rings (D6MRs), as shown in Fig. 2(a). The supercages of FAU appear among them, and are arrayed in a diamond structure by the sharing of 12-membered rings (12MRs); the double diamond structure is constructed of β -cages and supercages. Large spheres illustrate s -electron wave functions. K-cation-type LSX has the chemical formula $K_{12}Al_{12}Si_{12}O_{48}$ per β -cage (or supercage), and is abbreviated to K_{12} -LSX here. By the loading of guest alkali metal, clusters are formed at the supercages and/or β -cages, depending on the loading density per β -cage (or supercage), n , and the kind of alkali metals as well. When potassium metal is highly loaded into Na_4K_8 -LSX, Néel's N-type ferrimagnetism is observed, and is explained by the antiferromagnetic interaction between two non-equivalent magnetic sublattices of clusters at β -cages and supercages [14,15].

In sodalite, β -cages are arrayed in a body centered cubic structure by the sharing of 6-membered-rings (6MRs), as shown in Fig. 2(b), where large spheres illustrate s -electron wave functions. Na-cation-type so-

dalite with the chemical formula $\text{Na}_3\text{Al}_3\text{Si}_3\text{O}_{12}$ per β -cage can be obtained by the extraction of NaOH from as-synthesized sodalite, and is abbreviated to Na_3 -SOD here. By loading of one Na atom per β -cage (Na/Na_3 -SOD), an Na_4^{3+} cluster is stabilized in each β -cage. This material shows clear antiferromagnetism [16,17].

Electron-phonon interaction which can stabilize small polarons or bipolarons, plays an important role in magnetic properties and insulator-to-metal transition [18]. In the present paper, we will provide an overview of exotic magnetism, including those found in recent results. These properties are discussed in close relation to the strongly correlated electron system as well as electron-phonon interaction.

II. EXPERIMENTAL PROCEDURES

We used synthetic zeolite powders of zeolites A, LSX and sodalite. The ionic exchange for original zeolites was made in aqueous solutions. A complete dehydration of zeolite powder was done by heating at 500 °C for one day under high vacuum. Distilled alkali metals were sealed together with the above dehydrated zeolite powder in a glass tube and adsorbed into the zeolite powder at ≈ 160 °C. The average loading density n per cage was adjusted by the weight ratio of alkali-metal to zeolite. The DC magnetization was measured for sample powders kept in synthetic quartz glass tubes by using a SQUID magnetometer (MPMS-XL, Quantum Design). Diffuse reflectivity (r) at room temperature was measured for powder samples kept in glass tubes. The optical absorption spectra were obtained from the Kubelka-Munk transformation $(1 - r)^2/2r$ for rather weak absorption. The optical reflection spectra were obtained from the sum spectra of the reflectivity (R) and transmittance (T), $R + T = 4r/(1 + r)^2$ [2]. R can be obtained in the case where T is small enough to be neglected ($R \gg T$).

III. EXPERIMENTAL RESULTS AND DISCUSSION

1. K-loaded K_{12} -A (K_n/K_{12} -A)

From the optical spectra, we can describe the quantum electronic states of *s*-electrons localized in nanoclusters. The reflection spectra of K-loaded K_{12} -A are shown in Fig. 3(a). With increasing average loading density per α -cage, n , an increase and a decrease in the reflection band intensities around 1 eV are seen. They are assigned to successive *s*-electron occupations of the $1s$ state followed by the $1p$ state [2]. The bands around 1.5 ~ 2.0 eV are assigned to $1p$ - $1d$ transitions, in accordance with the

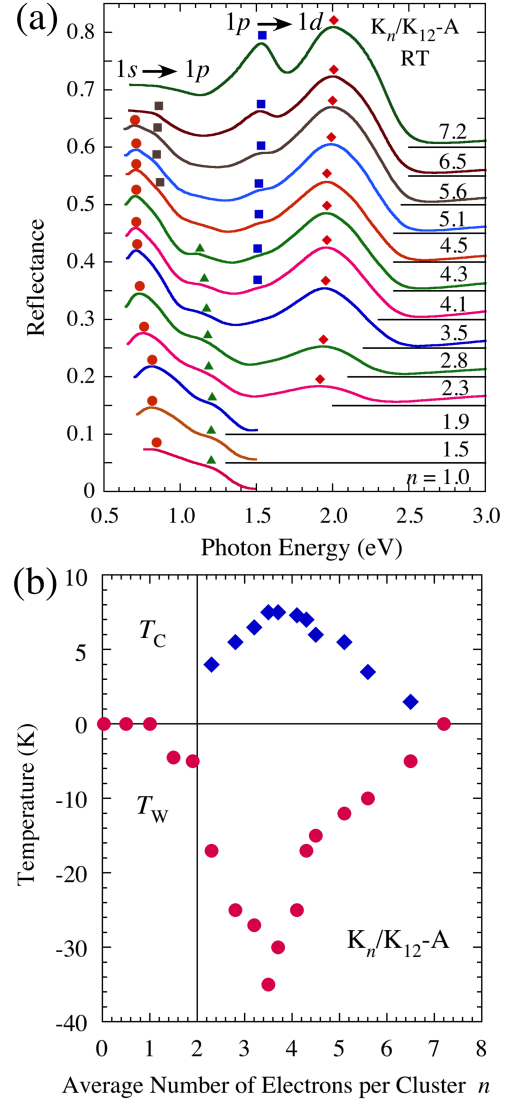


Fig. 3. (Color online) (a) Optical reflection spectra of K-loaded K_{12} -A (K_n/K_{12} -A) at the average loading density of K atoms per α -cage, n , and (b) Curie (T_C) and Weiss (T_W) temperatures in K_n/K_{12} -A.

electron occupation of the $1p$ state at $n > 2$. Fine structures are explained by the deviation from the spherical or cubic potential.

Spontaneous magnetization has only been observed at $n > 2$ [19], and the highest Curie temperature appears around $n \approx 3.6$ [5,20]. A remarkable decrease in the *g*-value has been observed in electron spin resonance (ESR) spectra for $n > 2$ [10], indicating that the orbital angular momentum at the $1p$ -like state contributes to the decrease in the *g*-value. The Jahn-Teller instability of $1p$ -like degenerate states can be suppressed by the large spin-orbit interaction [7,8]. The antiferromagnetic interaction has been expected from the negative Weiss temperature in the Curie-Weiss behavior of magnetic susceptibility [21, 22], where the mechanism of ferrimag-

netism was proposed tentatively. The n -dependences of Curie and Weiss temperatures in K_n/K_{12} -A are shown in Fig. 3(b), where the Curie and Weiss temperatures are estimated from the Arrott-plot analysis and the Curie-Weiss behavior, respectively. The origin of the spontaneous magnetization is newly proposed as the large-angle spin-canting mechanism of antiferromagnet [6], where the spin-orbit interaction is strongly enhanced by the degeneracy of the $1p$ -like orbital [7, 8, 10]. An anomalous increase in magnetization has been observed above ≈ 25 T, and amounts to more than $1 \mu_B$ per cluster [8]. In MuSR experiments, a rapid decay component has been observed by the Fermi-contact interaction of muons with electron spins, and is quickly decoupled by the very low longitudinal field [9]. This result is explained by the low field magnetization of electron spins by the spin-canting mechanism [9]. The Dzyaloshinsky-Moriya interaction is expected in case of no inversion symmetry at the center of 8MRs between adjacent clusters. In fact, the superlattice structure has been observed at $n > 2$, and non-equivalent cluster structures are expected to be arrayed alternatively [22, 23]. Large-angle spin-canting has been expected theoretically in the case of degenerate states [24]. Therefore, the lack of inversion symmetry and the degeneracy of the $1p$ -like state can explain the large-angle spin-canting mechanism.

According to the first-principles band calculation of K-loaded zeolite A in the simplified structure, the band structures are found to be quite simple and consistent with the tight-binding model formed by the $1s$ - and $1p$ -like electronic states of clusters [25, 26]. The unscreened Coulomb repulsion energy of two $1p$ -like electrons in the same cluster is estimated to be ≈ 4 eV. This value is much larger than the calculated value of the $1p$ -like bandwidth ≈ 0.4 eV. Hence, the assignment of Mott insulator is quite consistent with the theoretical expectation. *Ab initio* density functional calculations are performed in K-loaded zeolite A in more realistic structures [27]. Both the spin state and the electronic state are found to be highly sensitive to cation arrangement. The bonding state between adjacent non-equivalent clusters (σ -bonding) is proposed. The Hund coupling is calculated to be quite large, although the spin-triplet state ($s = 1$) has not been detected experimentally.

2. K-loaded Na_4K_8 -LSX ($\text{K}_n/\text{Na}_4\text{K}_8$ -LSX)

The electronic states of alkali metals in zeolite LSX are quite different from those in zeolite A. The main reason is the wide windows of supercages (12MRs) shown in Fig. 2(a). In the case of zeolite A, the distance between adjacent α -cages, the effective inside diameter of the α -cage and that of the 8MR are 12.3, 11 and ≈ 4.5 Å, respectively. In the case of LSX, the distance between adjacent supercages is 10.8 Å, which is smaller than the effective inside diameter of the supercage (13

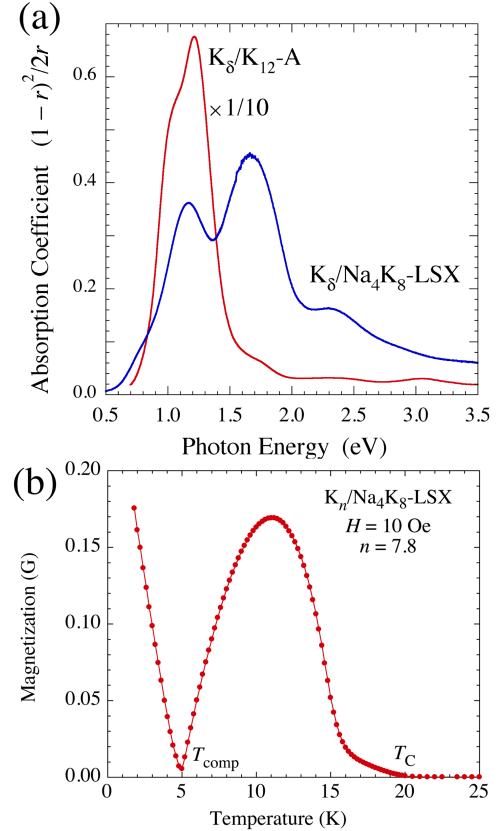


Fig. 4. (Color online) (a) Absorption spectra of dilutely K-loaded Na_4K_8 -LSX ($\text{K}_\delta/\text{Na}_4\text{K}_8$ -LSX, $\delta \ll 1$) and K_{12} -A ($\text{K}_\delta/\text{K}_{12}$ -A, $\delta \ll 1$), and (b) temperature dependence of magnetization in $\text{K}_{7.8}/\text{Na}_4\text{K}_8$ -LSX at an applied magnetic field of 10 Oe.

Å). The effective inside diameter of the 12MR between adjacent supercages is ≈ 8 Å. Hence, the supercages of LSX are larger and closer together than the α -cages of zeolite A. It is expected that electrons are not well localized in supercages and that the energy band width is wider than that in zeolite A. In fact, the absorption spectrum of dilutely K-loaded Na_4K_8 -LSX ($\text{K}_\delta/\text{Na}_4\text{K}_8$ -LSX, $\delta \ll 1$) contains wide absorption bands as shown in Fig 4(a). The absorption spectrum of dilutely K-loaded K_{12} -A ($\text{K}_\delta/\text{K}_{12}$ -A, $\delta \ll 1$) is shown for comparison. Spectral shape reflects the joint density of states for optically allowed transitions. The absorption spectrum for $\text{K}_\delta/\text{K}_{12}$ -A is simply assigned to the allowed transition from $1s$ - to $1p$ -like states, where the transition from $1s$ - to $1d$ -like states (expected at ≈ 2.7 eV in the spherical-well potential model with a diameter of 11 Å) is optically forbidden. The spectral shape of $\text{K}_\delta/\text{Na}_4\text{K}_8$ -LSX, however, has many bands and the total width is much wider than that of $\text{K}_\delta/\text{K}_{12}$ -A. If we assume T_d symmetry for the supercage, optical transitions are expected from the a_1 ground state (s -like) to two t_2 states which are p - and d -like states estimated to be at ≈ 0.86 eV and ≈ 1.9 eV higher than the a_1 state, respectively, in the spherical-

well potential model with a diameter of 13 Å. The *s*-, *p*- and *d*-like states can hybridize with each other in the T_d symmetry and have nearly continuous density of states.

The most striking result in K-loaded $\text{Na}_4\text{K}_8\text{-LSX}$ is the Néel's N-type ferrimagnetism [14,15]. When $n = 7.8$ ($\text{K}_{7.8}/\text{Na}_4\text{K}_8\text{-LSX}$), a clear zero-minimum of magnetization is observed at 5 K under an applied magnetic field of 10 Oe, as shown in Fig. 4(b). This temperature is called the compensation temperature, T_{comp} . In order to explain this result, two non-equivalent magnetic sublattices, namely the double diamond structure network of β -cages and supercages, must be assumed. If the bandwidth of electrons in a supercage network is wider than the limit of the Mott insulator, a metallic phase can be expected for supercage clusters. In fact, these materials are metallic at higher loading densities of K metal [18]. We can expect the density of states at the Fermi energy of the supercage cluster network to be high enough for a ferromagnetic or nearly ferromagnetic state. On the other hand, electrons in β -cages are well localized, and have a very weak mutual interaction with those in adjacent β -cages because the D6MRs between them widely separate the electron wave functions. However, electrons in β -cages can have a finite antiferromagnetic interaction with electrons in supercages through 6MRs shown in Fig. 2(a). This antiferromagnetic interaction may stabilize the ferromagnetic sublattice of the supercage cluster network. According to the above speculation, the supercage magnetic sublattice is expected to be magnetically ordered below the Curie temperature, followed by the magnetic ordering of the β -cage magnetic sublattice. With decreasing temperature, the β -cage magnetic sublattice grows rapidly and has the same (but opposite) magnetization with that of supercage magnetic sublattice at T_{comp} , indicating the zero minimum of magnetization. Below T_{comp} , the β -cage magnetic sublattice dominates the magnetization. The scheme of localized electrons of β -cages in the metallic network of the supercage electrons presents an interesting system such as the Kondo lattice, where the second electron at the β -cage can have higher energy than the Fermi energy [15]. Unlike in the ordinary Kondo regime, metallic electrons in the supercage cluster network are strongly correlated and spin-polarized.

When $n\text{Na}$ atoms are loaded into $\text{Na}_{12}\text{-LSX}$ ($\text{Na}_n/\text{Na}_{12}\text{-LSX}$), quite different electronic states are observed [28, 29]. The optical spectra show an insulating phase up to $n \approx 10$, but suddenly change to the metallic shape at $n \approx 12$ [28]. The electrical resistivity dramatically decreases by several orders of magnitude [29]. At the same time, a lot of paramagnetic moments are thermally excited. The insulating and non-magnetic phase at $n < 11$ is explained by the polaron effect, where even numbers of electrons are self-trapped by the strong electron-phonon interaction and small multiple-bipolarons in the spin-singlet state are stabilized. These small polarons are immobile because of a large lattice distortion of Na cations. At $n > 11$, multiple-bipolarons

become unstable due to the Coulomb repulsion of electrons, and large polarons in the metallic state are stabilized. Small polarons are thermally excited and can have paramagnetic properties. The anomalous paramagnetic behavior has been observed in NMR study of ^{23}Na [30]. This insulator-to-metal transition and thermal excitation of paramagnetic properties are explained by electron correlation as well as by electron-phonon interaction in the deformable space [29].

3. Na-loaded $\text{Na}_3\text{-SOD}$ ($\text{Na}/\text{Na}_3\text{-SOD}$) and Rb-loaded $\text{K}_3\text{-SOD}$ ($\text{Rb}/\text{K}_3\text{-SOD}$)

In sodalite, β -cages with an effective inside diameter of ≈ 7 Å are arrayed in a body centered cubic structure through the sharing of 6MRs having an effective inside diameter of ≈ 2.8 Å. Clear antiferromagnetism has been observed in $\text{Na}/\text{Na}_3\text{-SOD}$, where an Na_4^{3+} cluster is stabilized in each β -cage [16]. This material is in the Mott insulator phase. The β -cage has O_h symmetry, but the Na_4^{3+} cluster has T_d symmetry. An electron in Na_4^{3+} cluster is expected to have mutual overlapping with those in adjacent β -cages through 6MRs. A clear oscillation of MuSR signals has been observed below the Néel temperature of ≈ 50 K [17]. Antiferromagnetic resonance has been clearly observed in X-band [31] and high frequency ESR spectra [32]. The ESR spectra in X-band are shown in Fig. 5(a). From the analysis of the spectral shape, the anisotropy field is estimated to be $1 \sim 2$ Oe. This value is very small, indicating that a fairly ideal Heisenberg antiferromagnet is realized. This property is explained by the *s*-like character of an electron in an Na_4^{3+} cluster, and weak easy-plane type anisotropy is proposed. The spin density of this material is quite small compared to other magnetic materials, but the 001 magnetic reflection has been detected below the Néel temperature by neutron diffraction [33]. The appearance of this reflection can support the antiferromagnetic ordering of spins.

Theoretical calculations of alkali-metal clusters in sodalite have been vigorously performed [34]. According to these theoretical calculations, the potassium system has larger magnetic interaction than the sodium system. In fact, the Néel temperature increases systematically with heavier alkali metals, such as 80 K for $\text{Rb}/\text{K}_3\text{-SOD}$ [35]. A broad spectrum has been observed in ^{27}Al -NMR below the Néel temperature in $\text{K}/\text{K}_3\text{-SOD}$ [36]. Clear oscillations of MuSR signal have been observed in $\text{Rb}/\text{K}_3\text{-SOD}$ as shown in Fig. 5(b). The estimated internal magnetic field at the muon stopping site is 155 Oe at $T = 0$ K, which is much larger than 92 Oe in $\text{Na}/\text{Na}_3\text{-SOD}$. The increase in the field can not be explained by the point dipole model. The mechanism of the increase is discussed in terms of both the deviation from the spherical wave function and the increase in Fermi contact [35].

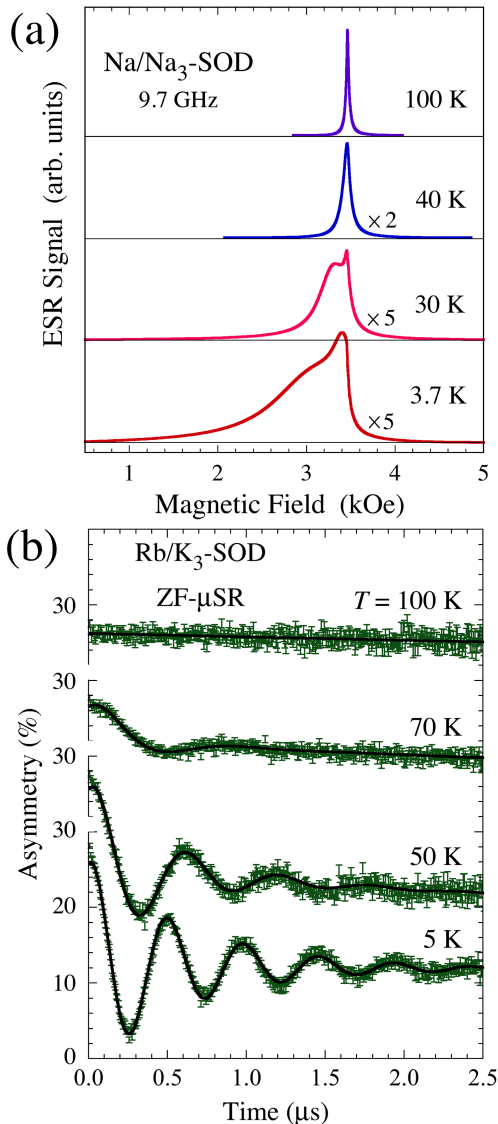


Fig. 5. (Color online) (a) X-band ESR spectra of antiferromagnet Na/Na₃-SOD at various temperatures. The Néel temperature is ≈ 50 K. (b) Zero-field MuSR spectra of antiferromagnet Rb/K₃-SOD at various temperatures. The Néel temperature is ≈ 80 K.

IV. CONCLUSION

The *s*-electrons provided into zeolites by the loading of guest alkali-metals have the localized natures of clusters in cages and strong electron correlation depending on the structure of the zeolite framework and the kind of alkali metals. These electrons have a mutual interaction and display exotic magnetic properties such as spin-canted antiferromagnetism in zeolite A and antiferromagnetism in sodalite. The Néel's ferrimagnetism observed in zeolite LSX indicates non-equivalent magnetic sublattices of supercages and β -cages.

ACKNOWLEDGMENTS

This work was supported by Grant-in-Aid for Scientific Research (24244059 and 19051009) and the G-COE Program (Core Research and Engineering of Advanced Materials-Interdisciplinary Education Center for Materials Science).

REFERENCES

- [1] R. Kubo, *J. Phys. Soc. Jpn.* **17**, 975 (1962).
- [2] T. Kodaira, Y. Nozue, S. Ohwashi, T. Goto and O. Terasaki, *Phys. Rev. B* **48**, 12245 (1993).
- [3] Y. Nozue, T. Kodaira and T. Goto, *Phys. Rev. Lett.* **68**, 3789 (1992).
- [4] Y. Nozue, T. Kodaira, S. Ohwashi, T. Goto and O. Terasaki, *Phys. Rev. B* **48**, 12253 (1993).
- [5] T. Nakano, Y. Ikemoto and Y. Nozue, *Eur. Phys. J. D* **9**, 505 (1999).
- [6] T. Nakano, D. Kiniwa, Y. Ikemoto and Y. Nozue, *J. Mag. Mag. Mat.* **272-276**, 114 (2004).
- [7] T. Nakano and Y. Nozue, *J. Comp. Meth. Sci. Engin.* **7**, 443 (2007).
- [8] T. Nakano, D. Kiniwa, A. Matsuo, K. Kindo and Y. Nozue, *J. Mag. Mag. Mat.* **310**, E295 (2007).
- [9] T. Nakano, J. Matsumoto, T. C. Duan, I. Watanabe, T. Suzuki, T. Kawamata, A. Amato, F. L. Pratt and Y. Nozue, *Physica B* **404**, 630 (2009).
- [10] T. Nakano, Y. Ikemoto and Y. Nozue, *J. Phys. Soc. Jpn.* **71**, Suppl. 199 (2002).
- [11] T. C. Duan, T. Nakano and Y. Nozue, *J. Mag. Mag. Mat.* **310**, 1013 (2007).
- [12] T. C. Duan, T. Nakano and Y. Nozue, *e-J. Sur. Scie. Nanotech.* **5**, 6 (2007).
- [13] T. C. Duan, T. Nakano, J. Matsumoto, R. Suehiro, I. Watanabe, T. Suzuki, T. Kawamata, A. Amato, F. L. Pratt and Y. Nozue, *Physica B* **404**, 634 (2009).
- [14] T. Nakano, K. Goto, I. Watanabe, F.L. Pratt, Y. Ikemoto and Y. Nozue, *Physica B* **374-375**, 21, (2006).
- [15] D. T. Hanh, T. Nakano and Y. Nozue, *J. Phys. Chem. Solids* **71**, 677 (2010).
- [16] V. I. Srdanov, G. D. Stucky, E. Lippmaa and G. Engelhardt, *Phys. Rev. Lett.* **80**, 2449 (1998).
- [17] R. Scheuermann, E. Roduner, G. Engelhardt, H.-H. Klauss and D. Herlach, *Phys. Rev. B* **66**, 144429 (2002).
- [18] T. Nakano, D. T. Hanh, N. H. Nam, Y. Owaki, S. Araki and Y. Nozue, to be published in *J. Kor. Phys. Soc.*
- [19] T. Nakano, Y. Ikemoto and Y. Nozue, *Mol. Cryst. Liq. Cryst.* **341**, 461 (2000).
- [20] T. Nakano, Y. Ikemoto and Y. Nozue, *J. Mag. Mag. Mat.* **226-230**, 238 (2001).
- [21] Y. Ikemoto, T. Nakano, Y. Nozue, O. Terasaki, S. Qiu, *Mater. Sci. Eng. B* **48**, 116 (1997)
- [22] Y. Maniwa, H. Kira, F. Shizu and Y. Murakami, *J. Phys. Soc. Jpn.* **68**, 2902 (1999).
- [23] T. Ikeda, T. Kodaira, F. Izumi, T. Ikeshoji and K. Oikawa, *J. Phys. Chem. B* **108**, 17709 (2004).
- [24] M. Tachiki, *J. Phys. Soc. Jpn.* **25**, 686 (1968).

- [25] R. Arita, T. Miyake, T. Kotani, M. Schilfgaarde, T. Oka, K. Kuroki, Y. Nozue and H. Aoki, *Phys. Rev. B* **69**, 195106 (2004).
- [26] H. Aoki, *Appl. Surf. Science* **237**, 2 (2004).
- [27] Y. Nohara, K. Nakamura and R. Arita, *Phys. Rev. B* **80**, 220410 (2009).
- [28] T. Nakano, T. Mizukane and Yasuo Nozue, *J. Phys. Chem. Solids* **71**, 650 (2010).
- [29] Y. Nozue, Y. Amako, R. Kawano, T. Mizukane and T. Nakano, *J. Phys. Chem. Solids* **73**, 1538 (2012).
- [30] M. Igarashi, T. Nakano, P. T. Thi, Y. Nozue, A. Goto, K. Hashi, S. Ohki, T. Shimizu, A. Krajnc, P. Jeglic and D. Arcon, *Phys. Rev. B* **87**, 075138 (2013).
- [31] T. Nakano, T. Kashiwagi, A. Hanazawa, K. Watanabe, M. Hagiwara and Y. Nozue, *J. Phys. Soc. Jpn.* **78**, 084723 (2009).
- [32] T. Kashiwagi, T. Nakano, A. Hanazawa, Y. Nozue and M. Hagiwara, *J. Phys. Chem. Solids* **71**, 544 (2010).
- [33] T. Nakano, M. Matsuura, A. Hanazawa, K. Hirota and Y. Nozue, *Phys. Rev. Lett.* **109**, 167208 (2012).
- [34] K. Nakamura, T. Koretsune and R. Arita, *Phys. Rev. B* **80**, 174420 (2009) and references therein.
- [35] T. Nakano, R. Suehiro, A. Hanazawa, K. Watanabe, I. Watanabe, A. Amato, F. L. Pratt and Y. Nozue, *J. Phys. Soc. Jpn.* **79**, 073707 (2010).
- [36] M. Igarashi, T. Nakano, A. Goto, K. Hashi, T. Shimizu, A. Hanazawa and Y. Nozue, *J. Phys. Chem. Solids* **71**, 638 (2010).